Hindawi Publishing Corporation
International Journal of Photoenergy
Volume 2014, Article ID 375746, 8 pages
http://dx.doi.org/10.1155/2014/375746

Research Article

Design of a Free-Ruthenium In_2S_3 Crystalline Photosensitized Solar Cell

Byeong Sub Kwak, Younghwan Im, and Misook Kang

Department of Chemistry, College of Science, Yeungnam University, Gyeongsan, Gyeongbuk 712-749, Republic of Korea

Correspondence should be addressed to Misook Kang; mskang@ynu.ac.kr

Received 13 March 2014; Revised 17 May 2014; Accepted 3 June 2014; Published 7 July 2014

Academic Editor: Antonio Otavio Patrocinio

A new type of sulfide-based, solid-state dye material that is sensitive to visible radiation was assessed as a potential replacement for commercial ruthenium complex dyes in a dye-sensitized solar cell (DSSC) assembly. The In_2S_3 crystals on the surface of the TiO_2 bottom blocking layer were grown as a solid-state dye material. Scanning electron microscopy of In_2S_3 revealed a microsized, 3D-connected sheet-like shape, which was confirmed by X-ray diffraction to be a beta-structure. The efficiency of the dye-sensitized solar cells assembled with a layer grown with In_2S_3 increased with increasing In_2S_3 mole concentrations to 0.05 M (1.02%) but decreased at concentrations greater than 0.6~0.8%. This suggests that crystalline In_2S_3 acts as a dye sensitized to visible radiation, but the short-circuit current density is too low compared to the commercially available ruthenium dye. This suggests that In_2S_3 crystals did not grow densely but were bulk-grown with large pores, resulting in a smaller amount of In_2S_3 per unit area. Two IPCE curves were observed, which were assigned to TiO_2 and In_2S_3, meaning that the TiO_2 surfaces were covered completely with In_2S_3 crystals. The exposure of TiO_2 eventually leads to a reaction with the electrolytes, resulting in lower quantum efficiency.

1. Introduction

The increasing demand for energy and the limited oil reserves have highlighted the need for the development of alternative forms of renewable energy. Solar energy is one option proposed to deal with the energy crisis because it is abundant, unlimited, and clean. Sunlight can be harvested and converted directly to electricity using photovoltaic devices [1–5]. Since O'Regan and Gratzel first reported dye-sensitized solar cells (DSSCs) in 1991 [6], there has been continuous research into DSSCs because of their numerous advantages over silicon solar cells, such as low cost, easy assembly, and relatively high efficiency [7–10]. DSSCs are one of the most promising methods for future large-scale energy production from renewable energy sources. DSSCs are composed of four major parts, a semiconducting cathode, Pt anode, iodine electrolyte, and photosensitive dye [11], which is the most important component. The photosensitizer, that is, the dye, in DSSCs should fulfill the following essential characteristics:

(1) the excited state energy level of the photosensitizer should be higher than that of the conduction band edge of the semiconductor;

(2) the absorption spectrum of the sensitizer should cover as much as of the visible light and even the near-infrared region as possible;

(3) the dye molecule should bind to the surface of the semiconductor efficiently through certain anchoring groups;

(4) the oxidized state level of the sensitizer should match the redox potential of the electrolyte;

(5) the sensitizer should be photo- and electrochemically and thermally stable.

Over the last 20 years, ruthenium (II) complexes based on carboxylic pyridine ruthenium compounds, such as N3 [12], N719 [13], N907 [14], and black dye [15], have shown a clear lead in the solar cell performance. The best solar-to-electricity

conversion efficiency of >10% was achieved using these ruthenium-complex photosensitizers. On the other hand, ruthenium-complex photosensitizers tend to deteriorate the lifespan of the cell, making the photosensitizers unstable under thermal stress and light soaking [16, 17].

Therefore, it is important to explore novel inorganic sensitizers composed of transition metals. Recently, as an alternative to dye sensitizers, narrow-band gap semiconducting quantum dots, such as CdS [18], CdSe [1], PbS [19], Sb_2S_3 [20], and $CuInS_2$ [21], have also been tested as photosensitizers. These cells are called quantum dot-sensitized solar cells (QDSSCs). The use of semiconductor QDs as sensitizers has the following advantages in solar cell applications over conventional dyes: possible tuning of the visible response by changing the QD size [22], large intrinsic dipole moment resulting from quantum confinement and a high extinction coefficient [23], possible multiple electron-hole pairs [24], and a potential theoretical maximum efficiency of 31% [25]. Although the above advantages are quite promising, the efficiencies of QDSSCs (typically below 5%) are much lower than that of DSSCs (ca. 10%). One of the reasons for the poor performance of QDSSCs is the difficulty in assembling the QDs on a mesoporous TiO_2 matrix to obtain a well-covered QD layer on the TiO_2 surface. Therefore, new metal sulfide materials including QDs, which are easier to manufacture, absorb visible light easily, and have excellent electron-transfer ability, are needed.

Although many studies have assessed a range of metal sulfide materials for solar cell applications, there are no reports of a detailed study of In_2S_3 for solar cell applications. Therefore, In_2S_3 was evaluated as a photosensitizer in this study. The In_2S_3 is an excellent electron donor, and three different structures are as follows: yellow α-In_2S_3 has a defect cubic structure; red β-In_2S_3 has a defect spinal, tetragonal structure; and γ-In_2S_3 has a layered structure. The β-form is believed to be the most stable form at room temperature. In addition, it is diamagnetic and exhibits n-type semiconductivity with an optical band gap of 2.1 eV [26]. In_2S_3 crystals are grown directly onto the surface of a TiO_2 seed layer electrode using a chemical bath deposition (CBD) method [27], and its photosensitive effect in DSSCs is discussed.

2. Experimental

2.1. In_2S_3 Crystals Grown over TiO_2 Seed Blocking Layers and Their Characterization. In_2S_3 crystals were grown on the surface of the TiO_2 seed blocking layer using a general CBD method [28]. First, a sol-gel dip-coating technique was used to fabricate a TiO_2 seed blocking layer onto a fluorine-doped tin oxide (FTO) conducting glass plate (Hartford, 30 ohm cm^{-2} and 80% transmittance in visible region). A FTO glass substrate, which covered one side with black tape, was dipped into a 0.1 M TTIP ethanol solution fixed at pH = 2.5 with acetic acid and aged for 24 h. The prepared TiO_2 blocking layer film was then annealed at 450°C for 30 minutes in air to remove the additives. In the secondary step, the In_2S_3 crystals were grown on the TiO_2 seed blocking layer using thiourea ($(NH_2)_2C$=S, 99.9%, Junsei Chemical, Japan) and indium chloride ($InCl_3$, 99.9%, Junsei Chemical, Japan) as the S and In precursors, respectively. Indium chloride (0.001~0.5 M) was dissolved in distilled water, and thiourea (0.0015~0.75 M) was then added slowly with stirring. The solution was fixed to pH = 2.5 using acetic acid. After stirring homogeneously for 2 h, the final solution was transferred to an autoclave, which included a TiO_2 seed blocking layered glass, and treated thermally at 80°C for 24 h. The resulting glass was washed with ethanol and dried at 60°C for 24 h. Here, a TiO_2 paste was not used. Instead, the TiO_2 seed blocking layer eventually acted as a working electrode.

2.2. Assembly of TiO_2 Seed Blocking/In_2S_3 Photosensitizer Layered-Solar Cells. To prepare a solar cell, a working TiO_2 seed blocking/In_2S_3 photosensitizer layered electrode was covered with a Pt-coated FTO counterelectrode, and the edges of the cell were sealed with a sealing sheet (PECHM-1, Mitsui-Dupont Polychemical) at 110°C. The used redox electrolyte consisted of 0.5 mol KI, 0.05 mol I_2, and 0.5 mol 4-tert-butylpyridine with an acetonitrile solvent. Sufficient electrolyte was injected into cells using a vacuum pump.

2.3. Characterization. The prepared TiO_2 (bottom)/In_2S_3 (top) films were examined by X-ray diffraction (XRD; MPD, PANalytical) using nickel-filtered CuKα radiation (40 kV, 30 mA). The surface morphology of the film was examined by scanning electron microscopy (SEM, S-4100, Hitachi). Cyclic voltammetry (CV, BAS 100B) of the TiO_2 and In_2S_3 powder disc was performed at room temperature at a scan rate of 100 mV s^{-1} in an electrolyte composed of 0.5 mol KI, 0.05 mol I_2, and 0.5 mol 4-tert-butylpyridine in acetonitrile. Platinum wire was used as the working and counterelectrodes, and Ag/AgCl was used as the reference electrode. The UV-visible (Cary 500 spectrometer) spectra of TiO_2 (bottom)/In_2S_3 (top) films were obtained using a reflectance sphere in the range, 200~800 nm.

The photovoltaic efficiency of the TiO_2 seed blocking/In_2S_3 photosensitizer layered-solar cells was calculated from the *I-V* curves that had been determined using a Sun 2000 solar simulator (ABET technology) equipped with a xenon lamp (max. 150 W). The light intensity of the solar simulator was equivalent to one sun at AM 1.5. The instrument was calibrated using a c-Si reference cell. The spectral output of the lamp was matched in the region, 350–800 nm, using a Schott KG-5 sunlight filter to reduce the mismatch between the simulated and true solar spectrum to less than 2%. The incident light intensity and active cell area were 100 mWcm^{-2} and 0.40 cm^2 (0.8 × 0.5 cm), respectively. The solar cell was measured at room temperature using a shading mask and the aperture area was used for the calculation. The major factors determining the efficiencies of the solar cells were the open-circuit voltage (V_{oc}), short-circuit current density (J_{sc}), and fill factor (FF).

Using the same equipment, the equilibrium conditions are important considerations in the IPCE measurements, where the spectral response is obtained under short-circuit conditions. In AC mode, the test SC was illuminated by monochromatic light with the addition of simulated AM 1.5 G

solar light to represent the solar cell working conditions. The photocurrent responding to monochromatic light was measured precisely using a lock-in amplifier at a frequency that was also applied to a mechanical chopper to modulate the monochromatic light. The total photocurrent could be estimated from the IPCE spectra by integrating the incident photon flux density, $I_{\text{photon}}(\lambda)$, and IPCE ($\lambda$) over the wavelength of incident light, which is expressed as [28]

$$J = q_e \int I_{\text{photon}}(\lambda) \cdot \text{IPCE}(\lambda)\, d\lambda, \quad (1)$$

where J is the photocurrent, q_e is the electron charge, and λ is the wavelength.

3. Results and Discussion

3.1. Physicochemical Properties of the TiO_2 Seed Blocking/In_2S_3 Photosensitizer Layered Film. Figure 1 shows XRD patterns of the prepared TiO_2 seed blocking/In_2S_3 photosensitizer (0.001, 0.01, 0.05, 0.1, and 0.5 M) layered films. Anatase TiO_2 [29] and tetragonal tin oxide [30] induced from the FTO glass were observed in the In_2S_3 film sample grown using the 0.001 M-In precursor, but no peaks were assigned to β-In_2S_3. On the other hand, with the exception of the 0.001 M-In precursor sample, all the diffraction peaks of the samples were indexed to β-In_2S_3 with a Fd-3m space group, which are in good agreement with the data reported in the literature [31]. Compared to the standard card, the relative intensities of the peaks at 14.3° (111 plane), 23.4° (220), 27.4° (311), 28.5° (222), 33.4° (400), 36.2° (331), 40.9° (422), 43.7° (511), 47.8° (440), 55.8° (533), 59.3° (444), 67.0° (731), 69.6° (800), 77.1° (751), 79.1° (840), and 88.9° (844) were obvious. The (311) XRD peak is normally the strongest. The mean crystalline sizes of the samples containing 0.001, 0.01, 0.05, 0.1, and 0.5 M of the In_2S_3 photosensitizer, which was calculated using Scherrer's equation, $D = \kappa\lambda/\beta\cos\theta$, were 48.10, 19.78, 36.21, 18.10, and 21.72 nm, respectively.

Figures 2(a) and 2(b) show a high-magnification SEM image (top view and side view) of the In_2S_3 crystals grown over the TiO_2 seed blocking layer. The TiO_2 seed blocking layer thickness was approximately 0.5 μm in all samples and the depths of the grown In_2S_3 crystals increased from 0.7 to 5.0 μm. The 3D-structured and connected sheet-like In_2S_3 particles were observed. According to the In_2S_3 concentration, the sheets on the top view were largely grown and the pore sizes were larger. The densities also increased with increasing In_2S_3 concentration to 0.05 M but decreased at concentrations >0.05 M.

Figures 3(a) and 3(b) present the UV-visible absorption spectra and Tauc's plot of the TiO_2 seed blocking/In_2S_3 photosensitizer (0.001, 0.01, 0.05, 0.1, and 0.5 M) layered films, respectively. This is a practical method for estimating the energy gap from an extrapolation of the absorption edge intercept on the x-axis or of that at the excitonic (shoulder) peak, called $\lambda_{1/2}$. The absorption spectra had a steeper absorption edge, which is similar to the results obtained from the Tauc equation [32]. The absorption band of the TiO_2 film normally appears at approximately 350 nm. According

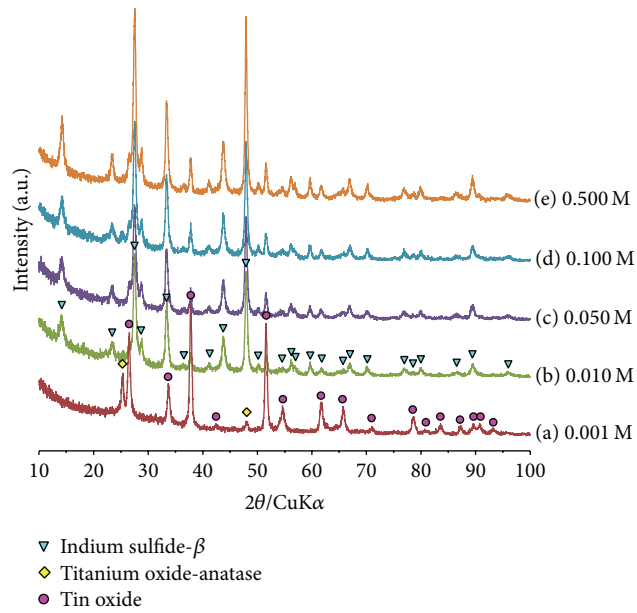

Figure 1: The XRD patterns of the prepared TiO_2 seed blocking/In_2S_3 photosensitizer (0.001, 0.01, 0.05, 0.1, and 0.5 M) layered films.

to the concentrations of the grown In_2S_3, the absorption bands shifted to a higher wavelength around the maximum, 450~650 nm. The band gap of semiconductor materials is closely related to the wavelength absorbed, where the band gap decreases with increasing absorption wavelength. The band gap can be calculated from the following Tauc equation: $(\alpha h\nu)^n = B(h\nu - E_g)$, where $h\nu$ is the photon energy, α is the absorption coefficient, B is a constant relative to the material, and the exponent n is a value that depends on the nature of the transition (2 for a direct allowed transition, 2/3 for a direct forbidden transition, and 1/2 for an indirect allowed transition). The band gap obtained by extrapolating the linear portion of the graph in the 0.05 M In_2S_3 photosensitizer layered on TiO_2 seed blocking (700 nm) was approximately 1.72 eV. In contrast, the TiO_2 seed blocking layered film had a band gap of 2.81 eV. Generally, the band gap of anatase TiO_2 is approximately 3.02 eV. On the other hand, the absorption in the visible region was attributed to the transition from the ground state to a few defects. This excitation character of the absorption spectra indicated the excellent crystal quality of the semiconductor. A redshift was observed in the optical absorption spectra of the TiO_2 hexagonal columns, which indicated that the TiO_2 particles showed quantum confinement related effects. This absorption in the visible region was attributed more to the transition from the ground state to a few defect-related deep states [33–35]: the value of E_g for bulk CdS was 2.5 eV, but a wide range of E_g values have been reported for CdS thin films depending mainly on the deposition technique. Evaporated CdS films with band gaps as low as 2.2 eV and chemically deposited CdS films with band gaps as high as 2.6 eV have been reported. These high E_g values for CdS have been attributed to quantum confinement effects due to the small grain size of the polycrystalline films.

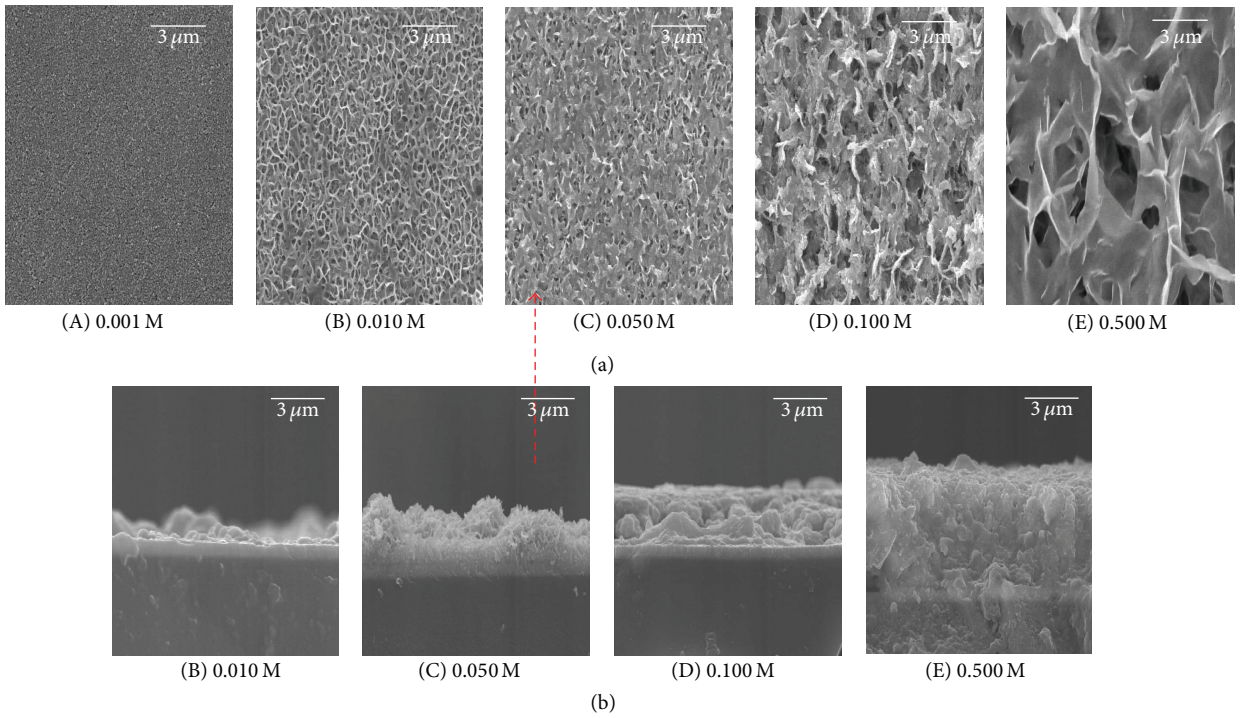

Figure 2: High-magnification SEM images (top view (a) and side view (b)) of the In_2S_3 crystals grown on TiO_2 seed blocking layer.

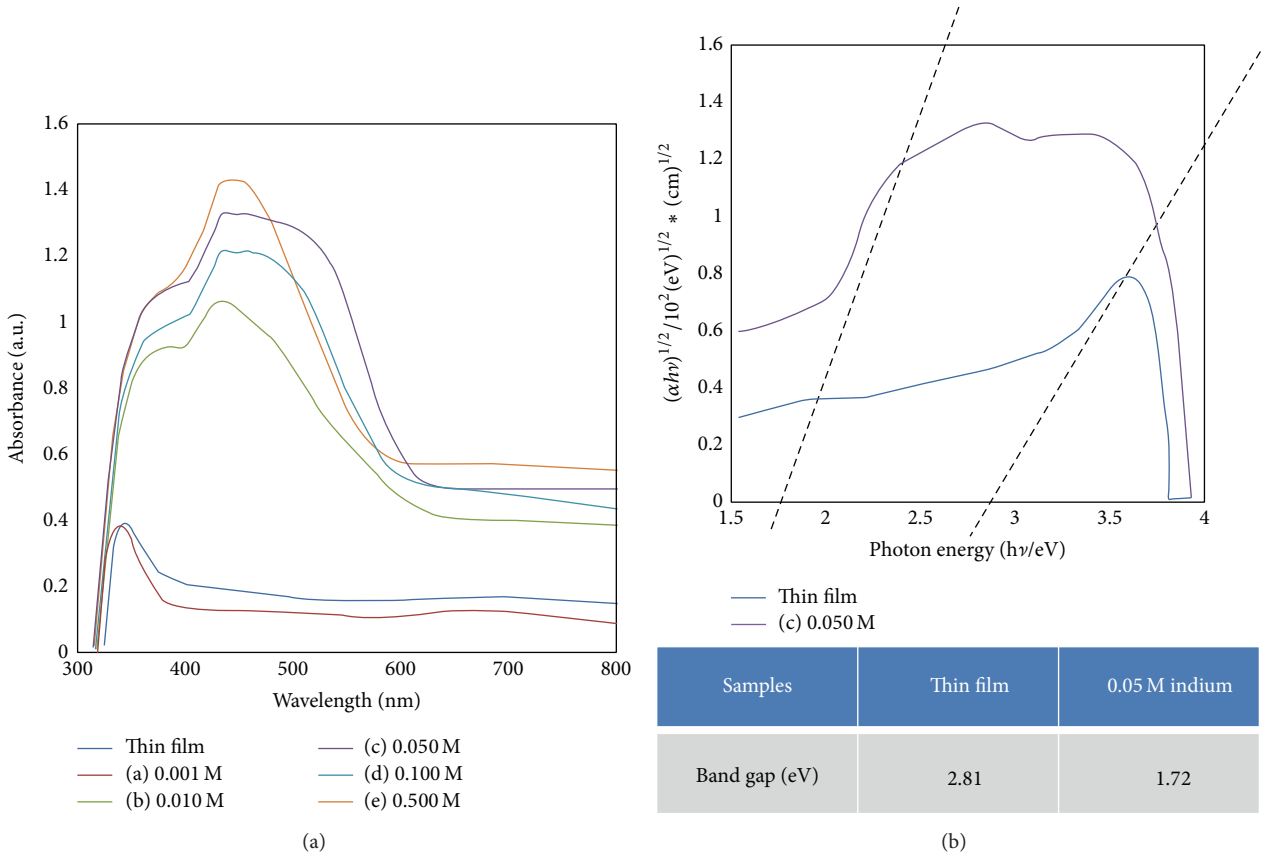

Samples	Thin film	0.05 M indium
Band gap (eV)	2.81	1.72

Figure 3: UV-visible absorption spectra (a) and Tauc's plots (b) of the TiO_2 seed blocking/In_2S_3 photosensitizer (0.001, 0.01, 0.05, 0.1, and 0.5 M) layered films.

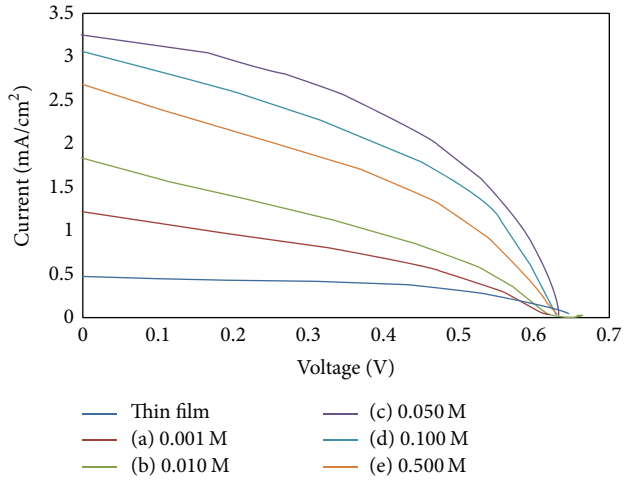

Sample	V_{oc} (V)	J_{sc} (mA/cm^2)	Fill factor	Efficiency y (%)
Thin film	0.65	0.52	0.58	0.20
(a) 0.001 M	0.61	1.38	0.43	0.36
(b) 0.010 M	0.62	1.95	0.40	0.48
(c) 0.050 M	0.63	3.31	0.49	1.02
(d) 0.100 M	0.62	3.13	0.41	0.80
(e) 0.500 M	0.62	2.79	0.38	0.66

FIGURE 4: I-V curve (up) and photovoltaic efficiencies (down) of the TiO_2 seed blocking/In_2S_3 photosensitizer layered-solar cells.

Consequently, the band gap can be varied according to the particle size or crystal defects. In addition, the band gap indicates that its electronic properties changed due to the small particle sizes of TiO_2, indicating that the energy of the lowest excited state of the sample and heat treatment depend on their size: the highest energy is reached at a smaller particle size. The band gap energies could be explained by the volume conservation law, which states that an increase in at least one lattice constant should be compensated for by a decrease in another and vice versa, as is the case in the low-energy regions. Therefore, anatase (2.81 eV) shows an almost linear decrease in the band gap with increasing volume or decreasing lattice constant. A smaller band gap is achieved by compressing the lattice constant [36, 37]. Because the semiconductor electrode plays an important role in accepting electrons and donating them to the solar cells, its light absorption is important. This suggests that In_2S_3 effectively absorbs a large range of visible light similar to commercial ruthenium dyes.

3.2. Photovoltaic Efficiency and Electronic Properties of the TiO_2 Seed Blocking/In_2S_3 Photosensitizer Layered-Solar Cells. Figure 4 shows the I-V curve (up) and photovoltaic efficiencies (down) of the TiO_2 seed blocking/In_2S_3 photosensitizer layered-solar cells. The TiO_2 nanoparticles typically used in DSSCs have a diameter of approximately 10~30 nm, through which it is easy for the long wavelengths of light to permeate.

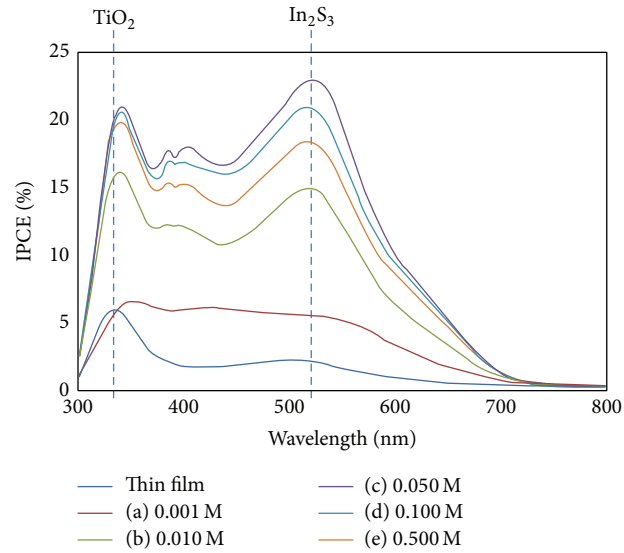

FIGURE 5: Incident photon-to-current conversion efficiencies of the TiO_2 seed blocking/In_2S_3 photosensitizer layered-solar cells.

Unfortunately, long-wavelength light is not used effectively in solar cells. In recent years, DSSCs assembled with a second layer film with a 4~5 μm thickness comprised of large nanoparticles or nanopores coated on the top of a dense TiO_2 electrode exhibited improved efficiency. The added second layer consisting of TiO_2, 400 nm in size, acts as a scattering material for increasing the incident light path, resulting in an array of photons that in turn improve the current density. This highlights the importance of the scattering materials in a DSSC assembly. On the other hand, a TiO_2 thick film as a second layer or scattering material was not used, and only a 0.5 μm TiO_2 seed blocking layer and 0.7~5 μm In_2S_3 photosensitizer layer were used. The 0.5 μm TiO_2 seed blocking layered-solar cell showed a power conversion efficiency of only 0.20% with V_{oc} = 0.65 V and J_{sc} = 0.52 mA/cm^2. This corresponds to the cell without a dye. On the other hand, the cases of the TiO_2 seed blocking/In_2S_3 photosensitizer layered-solar cells showed a higher J_{sc}. In particular, the current density increased until a In_2S_3 photosensitizer content of 0.05 M. The conversion efficiency was maximized to 1.20% in the TiO_2 seed blocking/0.05 M In_2S_3 photosensitizer layered-solar cell. This suggests that the In_2S_3 crystalline acts as a dye sensitized to visible radiation, even though the short-circuit current density is too small compared to the use of the commercially available ruthenium dye. This suggests that In_2S_3 crystals are not grown densely and are bulk-grown with rather large pores, resulting in the existence of a smaller amount of In_2S_3 per unit area. Moreover, the exposure of TiO_2 eventually leads to a reaction with the electrolytes and a smaller quantum efficiency. Chemical bath deposition provides a high surface coverage of crystals, but a lack of capping agents leads to a broad size distribution as well as a higher density of surface defects of crystals [38]. Therefore, a photoanode with a high crystal loading, fewer surface traps,

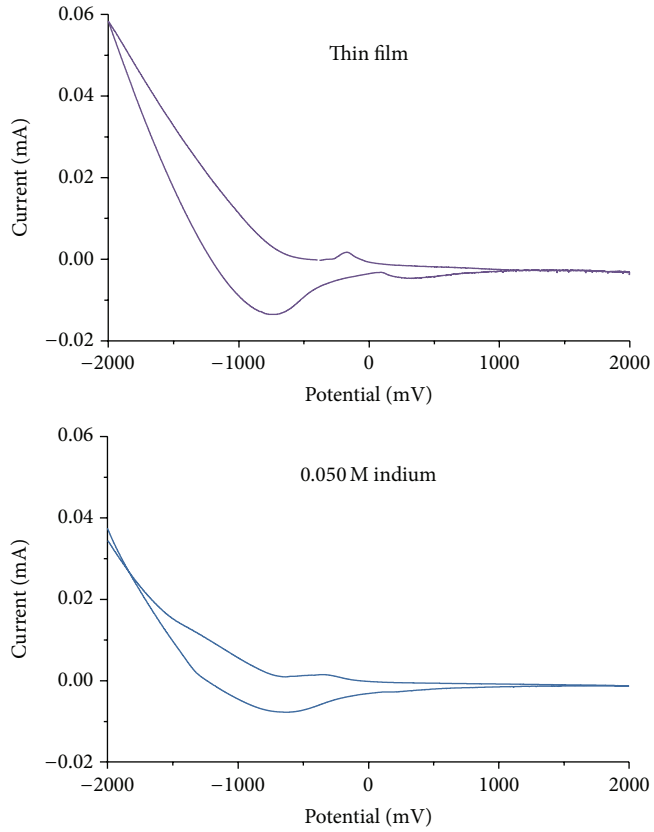

Samples	Thin film	0.05 M indium
LUMO (mV)	−4.191	−3.970
Epc (mV)	−189.3	−410.5

Figure 6: Cyclic voltammetry measurements of the TiO_2 and In_2S_3 pellets.

and strong crystals/TiO_2 electronic coupling is essential for constructing highly efficient solar cells.

The incident photon-to-current conversion efficiencies (IPCE) in Figure 5 indicate the number of incident photons inside the cell as well as their contribution to the conversion efficiency. The commercial ruthenium dyes used in general DSSCs that respond primarily to the wavelength of visible light were measured in the region, 300~750 nm, and reacted at approximately 530 nm, showing the highest quantum number (≈60~80%) [39]. Two IPCE curves were observed, which were assigned to TiO_2 and In_2S_3 at a maximum of 320 and 520 nm, respectively, and the curves increased with increasing In_2S_3 concentration. On the other hand, the quantum efficiencies were smaller than those of the commercial ruthenium dyes because the TiO_2 surfaces were not covered perfectly with In_2S_3 crystals. Eventually, the quantum efficiency for visible radiation decreased. The solar cell assembled with a 0.05 M In_2S_3 dye layer showed a maximum quantum efficiency of 22%, resulting in a lower solar conversion to electron efficiency ratio.

Figure 6 shows the cyclic voltammetry measurements for the TiO_2 and In_2S_3 pellets. In the present study, the oxidation potentials were measured by cyclic voltammetry in distilled water solutions. The pelletized samples were used as the working electrodes, Ag/AgCl was used as the reference electrode, and 0.1 M KCl was used as the supporting electrolyte. A reversible wave is needed for the absolute potentials between the reduction (E_{pc}) and oxidation peaks (E_{pa}). When such reversible peaks are observed, thermodynamic information in the form of a half cell potential $E^0_{1/2}$ can also be determined [40]. Recently, some studies devised a useful equation based on cyclic voltammetry for determining the HOMO and LUMO energy levels. The ferrocene ($E_{1/2}$ versus Ag/Ag^+ = +0.42 eV) potential, which is used as a standard, should be measured in the electrolyte solution using the same reference electrode, with a fixed −4.8 eV energy level in the vacuum set. The HOMO or LUMO energy levels can be calculated using the following formula: HOMO (or LUMO) (eV) = $-4.8 - (E_{onset} - E_{1/2(Ferrocene)})$ or E_g (= band gap) = HOMO-LUMO. Here, E_{onset} is the starting point of the redox potential, which was used more often than the peak potential value. In synthesized TiO_2, the Ti(IV) → Ti(0) redox reaction appears reversible, and the absolute reduction potential (E_{pc}) was observed at −189.3 mV. Using the Ag/AgCl reference electrode, the onset potential for reduction was determined for In_2S_3 powder and was −410.5 mV. Therefore, the corresponding LUMO energy levels for TiO_2 and In_2S_3 were calculated to be −4.191 and −3.970 eV, respectively. Consequently, these values could change to −0.31 and −0.53 eV depending on the upper equation. In DSSCs, the potential location of the conduction band is more important than the band gap of the semiconductor electrode because it should always be lower than the LUMO level of the dye (normally by 0.2 eV).

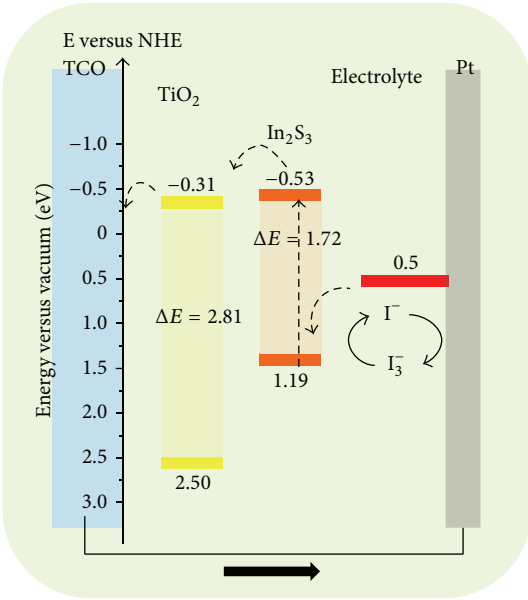

Scheme 1: Model for the potential energy diagram expected from the results of the CV curves and UV-visible spectra.

A model of the potential energy diagram was suggested from the CV curves and UV-visible spectra, as shown in Scheme 1. The conduction band of the TiO_2 blocking layer was located at slightly (0.22 eV) lower energy levels than the LUMO level of the In_2S_3 dye. This suggests that electrons donated from the LUMO of the In_2S_3 dye are transferred easily to the conduction band of the TiO_2 film with less electron loss. The transferred electrons can move easily to the external circuit through the TCO electrode.

4. Conclusions

In this study, β-type In_2S_3 crystals with various concentrations were grown on the surface of the TiO_2 bottom blocking layer by CBD. The grown In_2S_3 crystals were applied to dye-sensitized solar cells as a solid dye. Micron-sized, 3D-connected sheet-like shapes were observed by SEM. The efficiency of the dye-sensitized solar cells prepared from the 0.05 M-In_2S_3 crystals was the highest at 1.02%. Two IPCE curves were observed, which were assigned to TiO_2 and In_2S_3, respectively. This means that the TiO_2 surfaces are not perfectly covered with In_2S_3 crystals. The exposure of TiO_2 can lead to a reaction with the electrolyte, resulting in an increase in resistance, an interruption of current flow, and a decrease in photoelectric efficiency. These results confirmed that the performance in DSSCs relies on a complete coating method. Therefore, more reliable coating methods will be needed to improve the efficiency.

Conflict of Interests

The authors declare that there is no conflict of interests regarding the publication of this paper.

Acknowledgment

This work was supported by 2013 the Innopolis Daegu Project, Research and Development Special Zones, Republic of Korea, for which the authors are very grateful.

References

[1] A. Shah, P. Torres, R. Tscharner, N. Wyrsch, and H. Keppner, "Photovoltaic technology: the case for thin-film solar cells," *Science*, vol. 285, no. 5428, pp. 692–698, 1999.

[2] A. Hiroki, P. Klaus, S. P. S. Milo, H. W. Alan, and H. F. Richard, "Composites of carbon nanotubes and conjugated polymers for photovoltaic devices," *Advanced Materials*, vol. 11, no. 15, pp. 1281–1285, 1999.

[3] M. C. Kevin and D. M. Michael, "Conjugated polymer photovoltaic cells," *Chemistry of Materials*, vol. 16, p. 23, 2004.

[4] M. A. Martínez, J. Herrero, and M. T. Gutiérrez, "Deposition of transparent and conductive Al-doped ZnO thin films for photovoltaic solar cells," *Solar Energy Materials and Solar Cells*, vol. 45, no. 1, pp. 75–86, 1997.

[5] G. Yu, J. Gao, J. C. Hummelen, F. Wudl, and A. J. Heeger, "Polymer photovoltaic cells: enhanced efficiencies via a network of internal donor-acceptor heterojunctions," *Science*, vol. 270, no. 5243, pp. 1789–1791, 1995.

[6] B. O'Regan and M. Gratzel, "A low-cost, high-efficiency solar cell based on dye sensitized colloidal TiO_2 films," *Nature*, vol. 353, pp. 737–740, 1991.

[7] S. Y. Huang, G. Schlichthorl, A. J. Nozik, M. Gratzel, and A. J. Frank, "Kinetics for the recombination of phenyl radicals," *The Journal of Physical Chemistry B*, vol. 101, pp. 14–18, 1997.

[8] G. K. Mor, K. Shankar, M. Paulose, O. K. Varghese, and C. A. Grimes, "Use of highly-ordered TiO_2 nanotube arrays in dye-sensitized solar cells," *Nano Letters*, vol. 6, no. 2, pp. 215–218, 2006.

[9] M. Gratzel, "Conversion of sunlight to electric power by nanocrystalline dyesensitized solar cells," *Journal of Photochemistry and Photobiology A*, vol. 164, no. 1–3, pp. 3–14, 2004.

[10] M. Gratzel, "Dye-sensitized solar cells," *Journal of Photochemistry and Photobiology C*, vol. 4, pp. 145–153, 2003.

[11] N. Robertson, "Optimizing dyes for dye-sensitized solar cells," *Angewandte Chemie International Edition*, vol. 45, pp. 2338–2345, 2006.

[12] R. Katoh, A. Furube, T. Yoshihara et al., "Efficiencies of electron injection from excited N_3 dye into nanocrystalline semiconductor (ZrO_2, TiO_2, ZnO, Nb_2O_5, SnO_2, In_2O_3) films," *Journal of Physical Chemistry B*, vol. 108, no. 15, pp. 4818–4822, 2004.

[13] W. Zhong-Sheng, K. Hiroshi, K. Takeo, and A. Hironori, "Significant influence of TiO_2 photoelectrode morphology on the energy conversion efficiency of N719 dye-sensitized solar cell," *Coordination Chemistry Reviews*, vol. 248, pp. 1381–1389, 2004.

[14] P. Wang, B. Wenger, R. Humphry-Baker et al., "Charge separation and efficient light energy conversion in sensitized mesoscopic solar cells based on binary ionic liquids," *Journal of the American Chemical Society*, vol. 127, no. 18, pp. 6850–6856, 2005.

[15] M. K. Nazeeruddin, P. Pechy, and M. Gratzel, "Efficient panchromatic sensitization of nanocrystalline TiO_2 films by a black dye based on atrithiocyanato-ruthenium complex ," *Chemical Communications*, vol. 1997, no. 18, pp. 1705–1706, 1997.

[16] C. Li, C. Su, H. Wang et al., "Design and development of cyclometalated ruthenium complexes containing thiophenyl-pyridine ligand for dye-sensitized solar cells," *Dyes and Pigments*, vol. 100, no. 1, pp. 57–65, 2014.

[17] G. J. Wilson and G. D. Will, "Density-functional analysis of the electronic structure of tris-bipyridyl Ru(II) sensitisers," *Inorganica Chimica Acta*, vol. 363, pp. 1627–1638, 2010.

[18] D. J. Kim, Y. M. Yu, J. W. Lee, and Y. D. Choi, "Investigation of energy band gap and optical properties of cubic CdS epilayers," *Applied Surface Science*, vol. 254, pp. 7522–7526, 2008.

[19] S. Thangavel, S. Ganesan, S. Chandramohan, P. Sudhagar, Y. S. Kang, and C. Hong, "Band gap engineering in PbS nanostructured thin films from near-infrared down to visible range by in situ Cd-doping," *Journal of Alloys and Compounds*, vol. 495, no. 1, pp. 234–237, 2010.

[20] V. P. Zakaznova-Herzog, S. L. Harmer, H. W. Nesbitt, G. M. Bancroft, R. Flemming, and A. R. Pratt, "High resolution XPS study of the large-band-gap semiconductor stibnite (Sb2S3): structural contributions and surface reconstruction," *Surface Science*, vol. 600, no. 2, pp. 348–356, 2006.

[21] G. Chen, L. Wang, X. Sheng, H. Liu, X. Pi, and D. Yang, "Chemical synthesis of Cu(In) metal inks to prepare $CuInS_2$ thin films and solar cells," *Journal of Alloys and Compounds*, vol. 507, pp. 317–321, 2010.

[22] A. Kongkanand, K. Tvrdy, K. Takechi, M. Kuno, and P. V. Kamat, "Quantum dot solar cells. Tuning photoresponse through size and shape control of CdSe-TiO_2 architecture," *Journal of the American Chemical Society*, vol. 130, no. 12, pp. 4007–4015, 2008.

[23] I. Moreels, K. Lambert, D. De Muynck et al., "Composition and size-dependent extinction coefficient of colloidal PbSe quantum dots," *Chemistry of Materials*, vol. 19, no. 25, pp. 6101–6106, 2007.

[24] L. Jonsson, M. M. Steiner, and J. W. Wilkins, "Coherent electron–hole correlations in quantum dots," *Applied Physics Letters*, vol. 70, no. 9, p. 1140, 1997.

[25] R. Windisch, P. Heremans, A. Knobloch et al., "Light-emitting diodes with 31% external quantum efficiency by outcoupling of lateral waveguide modes," *Applied Physics Letters*, vol. 74, article 2256, 1999.

[26] N. Barreau, S. Marsillac, D. Albertini, and J. C. Bernede, "Structural, optical and electrical properties of β-In2S3-3xO3x thin films obtained by PVD," *Thin Solid Films*, vol. 403-404, pp. 331–334, 2002.

[27] C. D. Lokhande, A. Ennaoui, P. S. Patil et al., "Chemical bath deposition of indium sulphide thin films: preparation and characterization," *Thin Solid Films*, vol. 340, no. 1, pp. 18–23, 1999.

[28] M. K. Nazeeruddin, A. Kay, I. Rodicio et al., "Solvation changes accompanying proton transfer from a carbon acid to alkoxide bases as revealed by kinetic isotope effects," *Journal of the American Chemical Society*, vol. 115, pp. 14–20, 1993.

[29] N. Serpone, D. Lawless, and R. Khairutdinov, "Size effects on the photophysical properties of colloidal anatase TiO_2 particles: size quantization or direct transitions in this indirect semiconductor?" *Journal of Physical Chemistry*, vol. 99, no. 45, pp. 16646–16654, 1995.

[30] R. G. Pavelko, F. Gispert-Guirado, and E. Llobet, "Parametric line profile analysis for in situ XRD of SnO*2* materials: separation of size and strain contributions," *Solid State Ionics*, vol. 255, pp. 21–29, 2014.

[31] S. Cingarapu, M. A. Ikenberry, D. B. Hamal, C. M. Sorensen, K. Hohn, and K. J. Klabunde, "Transformation of indium nanoparticles to β-indium sulfide: digestive ripening and visible light-induced photocatalytic properties," *Langmuir*, vol. 28, no. 7, pp. 3569–3575, 2012.

[32] J. Tauc, R. Grigorovich, and A. Vancu, "Optical properties and electronic structure of amorphous germanium," *Physica Status Solidi*, vol. 15, no. 2, pp. 627–637, 1966.

[33] K. L. Narayanan, K. P. Vijayakumar, K. G. M. Nair, N. S. Thampi, and K. Krishan, "Structural transformation of dip coated CdS thin films during annealing," *Journal of Materials Science*, vol. 32, no. 18, pp. 4837–4840, 1997.

[34] D. Lincot, B. Mokili, M. Froment et al., "Phase transition and related phenomena in chemically deposited polycrystalline cadmium sulfide thin films," *Journal of Physical Chemistry B*, vol. 101, no. 12, pp. 2174–2181, 1997.

[35] M. B. Ortuno-Lopez, M. Sotelo-Lerma, A. Mendoza-Galvan, and R. Ramirez-Bon, "Optical band gap tuning and study of strain in CdS thin films," *Vaccum*, vol. 76, no. 2-3, pp. 181–184, 2004.

[36] H. Mathieu, J. Pascual, and J. Camassel, "Uniaxial stress dependence of the direct-forbidden and indirect-allowed transitions of TiO_2," *Physical Review B*, vol. 18, no. 12, pp. 6920–6929, 1978.

[37] H. Lin, C. P. Huang, W. Li, C. Ni, S. Ismat Shah, and Y.-H. Tseng, "Size dependency of nanocrystalline TiO_2 on its optical property and photocatalytic reactivity exemplified by 2-chlorophenol," *Applied Catalysis B: Environmental*, vol. 68, no. 1, pp. 1–11, 2006.

[38] P. K. Nair, M. T. S. Nair, V. M. Garcia et al., "Semiconductor thin films by chemical bath deposition for solar energy related applications," *Solar Energy Materials and Solar Cells*, vol. 52, no. 3-4, pp. 313–344, 1998.

[39] M. Zalas, B. Gierczyk, M. Klein, K. Siuzdak, T. Pedzinski, and T. Łuczak, "Synthesis of a novel dinuclear ruthenium polypyridine dye for dye-sensitized solar cells application," *Polyhedron*, vol. 67, p. 381, 2014.

[40] J. Kim, H. Lee, and M. Kang, "Newly designed dye-sensitized solar cells fabricated with double-layered TiO_2 (bottom layer)/B_x-TiO_2 (top layer) combined electrodes for improved photocurrent," *Solar Energy*, vol. 86, no. 9, pp. 2862–2870, 2012.